Atomic Data Needs for X-ray Astronomy. 22 June 2000
http://heasarc.gsfc.nasa.gov/docs/heasarc/atomic/
M. A. Bautista, T. R. Kallman, and A. K. Pradhan, eds.

First Results of the Chandra-LETGS

P. Predehl, B. Aschenbach H. Bräuninger, W. Burkert, V. Burwitz, G. Hartner, J. Trümper

Max-Planck-Institut für Extraterrestrische Physik (MPE), Postfach 1603, D-85740 Garching, Germany

J.H.M.M. Schmitt

Universität Hamburg, Gojenbergsweg 122, D-21029 Hamburg, Germany

A.C. Brinkman, C.J.T. Gunsing, J.S. Kaastra, R.L.J. van der Meer, R. Mewe, F. Paerels [1], J.J. van Rooijen

Space Research Organization of the Netherlands (SRON), Sorbonnelaan 2, 3584 CA Utrecht, The Netherlands

J.J. Drake, O. Johnson, M. Juda, S.S. Murray, D. Pease, P. Ratzlaff, B.J. Wargelin

Harvard-Smithsonian Center for Astrophysics, 60 Garden Street, Cambridge, MA 02138, USA

Abstract. We present the first results obtained with the Low Energy Transmission Grating Spectrometer (LETGS) onboard the Chandra X-ray Observatory. The LETGS covers the wavelength range between 5 and 175 Å (2.5–0.07 keV) with a spectral resolution of about 0.06 Å. A number of calibration measurements were carried out in order to determine the instrument's performance, i.e., spectral resolution, the wavelength scale accuracy, and the effective area. The spectral resolution of the instrument, dominated by the angular resolution of the mirror, is as specified and predicted on the basis of preflight measurements. The calibration of the effective area is still an ongoing process. A serious problem for the LETGS is the high background of the HRC-S detector which serves as readout of the grating spectra. The 'First Light' observation of the star Capella shows a beautiful line-rich spectrum. He-like triplet diagnostics could be applied for the first time to a star other than the Sun.

1. Instrument Description

The Chandra X-ray Observatory was successfully launched on July 23, 1999. As the last of four instruments, the Low Energy Transmission Grating Spectrometer (LETGS) was inserted into the telescope beam on September 6, 1999.

The LETGS consists of three subsystems: the High Resolution Mirror Assembly (HRMA) Van Speybroeck et al.(1997), the Low Energy Transmission Grating (LETG) Brinkman et al.(1987), Brinkman et al.(1997), Predehl et al.(1997), and the High Resolution Camera for spectroscopy (HRC-S) Murray et al.(1997). The LETG has been designed and manufactured in Europe in a collaborative effort between SRON in the Netherlands and MPE in Germany, and consists of a toroidally shaped ring-structure, covered with 540 grating elements. Each element with a diameter of 1.5-cm carries a gold-wire grating with a line density of 1008 lines/mm. The grating wires are held only by a coarse support structure but not by a substrate in order to avoid instrumental absorption features. The elements are mounted with their centers on the Rowland torus and with their planes perpendicular to the incoming X-ray beam (the LETG is placed in the convergent beam just behind the mirror system). For X-rays falling onto the center of the grating elements, the dispersed images are sharp. However, the finite size of the elements

[1] Present address, Columbia University, New York, NY, USA

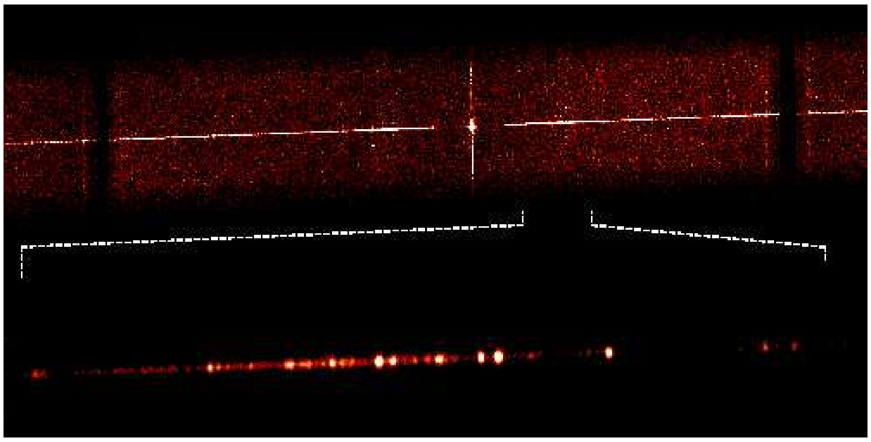

Figure 1. The raw detector image of the HRC-S detector. For the sake of clarity, only the center plate and small parts of the outer plates are shown. The dispersion is along the horizontal direction, and diffraction by the fine support grid is seen in the cross-dispersion direction. The faint hexagonal pattern around the 0^{th}-order is from diffraction by the coarse support grid. Underneath an extracted region from 12 Å to 23 Å with the strong Fe XVII and the oxygen triplet (at the right end) is shown.

causes a slight widening of the image particularly at longer wavelengths. The spectrum dispersed by the LETG behind the telescope forms an image in the focal plane with the zeroth order at the focus position and the plus and minus first and higher orders symmetrically on either side of it (see Figure 1). The prime detector to read out the LETG spectrum is the HRC-S detector. It consists of three flat segments, each 10 cm long and 2 cm wide. The outer segments are tilted with respect to the center one in order to approximate the Rowland circle. The dispersion is 1.15 Å/mm in first spectral order and is determined by the system geometry and the grating line density. Both are optimized in order to cover the wavelength range between 5 and 175 Å (2.5–0.07 keV). The detector can be moved in the cross-dispersion direction and along the optical axis in order to optimize the focus for spectroscopy. The nominal zero order point focus on the central detector plate is displaced by 4 mm with respect to the center along the dispersion direction. This asymmetry is created in order to avoid that the two small dead areas between the center detector strip and the outer plates block the same spectral band.

2. Data Analysis

The spectral width in the cross-dispersion direction is minimal at the zeroth order and fans out towards larger wavelengths, due to the intrinsic astigmatism of a Rowland circle spectrograph. The extraction of the spectrum from the image is done by applying a spatial filter and constructing a histogram of counts vs. position along the dispersion direction. The background of the HRC-S is rather high due to a malfunction of the anti-coincidence circuit in the HRC-S. Fortunately, the background is fairly uniform over the entire detector area. Therefore it can be reliably estimated from areas on the detector away from the spectral image. The width w (in cross dispersion direction) of the spatial filter can be optimized in order to get a maximum signal-to-noise ratio according to

$$\frac{S}{N}(w) = \frac{M - B}{\sqrt{M + B}} \tag{1}$$

with M the measured intensity spatially filtered from the spectrum (source+background) and B the intensity filtered from a background region having the same extent in cross dispersion direction. Both M and B depend, of course, on the width w of the extracted region. The slight influence on the effective area can be easily modeled because the intensity profile in cross dispersion direction is well known: in its outer part it is dominated by the dispersion by the coarse support structure, in its inner part it is simply the point response function of the mirror system.

The detector gain varies strongly over the detector area, a behavior which is not sufficiently well calibrated. We have applied a pulse height filter in order to further suppress the background. However, this has a significant influence on the effective area of the instrument as measured on ground. Therefore, we have done all analyses without applying this filter so far, but work is going on to optimize also this kind of background reduction.

Unlike the High Energy Transmission Grating Spectrometer (HETGS), the LETGS is not able to separate higher diffraction order lines. So far it does not seem to be a serious problem to distinguish between first and higher order lines because of the high spectral resolution of the instrument which allows to separate lines easily and the fact that the relative efficiencies of the higher orders with respect to the first one is well calibrated at several wavelengths.

3. First Light Spectrum

Capella is a binary system at a distance of 12.9 pc comprising G8 and G1 giants with an orbital period of 104 days (Hummel et al. 1994). It is the brightest quiescent coronal X-ray source in the sky after the Sun, and is therefore an obvious line source candidate for first light and for instrument calibration. X rays from Capella were discovered in 1975 by Catura et al.(1975), Mewe et al.(1975) and subsequent satellite observations provided evidence for a multi-temperature component plasma (e.g. Mewe(1991) for references). The most recent prior spectrum was obtained with EUVE, longward of 70 Å with a resolution of about 0.5 Å (Dupree et al. 1993; Schrijver et al. 1995).

The LETG First Light observation on Capella was performed on 6 September 1999 (00h27m UT – 10h04m UT) with LETG and HRC-S. The observation time was $\sim$ 34 ksec (see Figure 1). The HRC-S output was processed through the standard pipeline processing, producing a FITS-file with detector positions, pulse height information, and wavelengths.

Figure 1 shows a detector image after it has been corrected for spacecraft attitude drift and dithering (controlled spacecraft movement in order to avoid that a point source illuminates a single pixel). The bright horizontal line is the dispersed spectrum, which is symmetrical around the zeroth order. Using the procedures described above, we could extract a beautiful, line-rich spectrum of Capella: almost 150 spectral lines (single side, including higher diffraction orders) could be identified. These lines were used for both calibration and scientific purposes (see Figure 2).

4. Wavelength Scale Calibration

For the complete HRC-S, the Capella spectrum has been analyzed in terms of the quantity $m\lambda_{observed} - m\lambda_{predicted}$ as a function of wavelength. The analysis involves 171 lines in the data set, and relates to both positive and negative orders. We tried to analyze the above quantity in terms of decenter (of the 0^{th} order along the dispersion axis), plate scale (conversion pixel or angle to wavelength) for the central detector element, off-sets (jumps) at the detector boundaries, and plate scales (or inclination angles) for the outer elements.

The procedure is as follows. First the centroid of 'unblended lines' was determined by a quasi-automatic fitting procedure. Then, the line was identified using existing literature. In addition to statistical errors on the line centroids, we also included an uncertainty to the theoretical wavelength (0.001 Å for the H and He-like lines, 0.003 Å for other lines with $\lambda < 20$ Å, all other lines 0.01 Å, and for higher orders m times the first order error). We fitted straight lines to the data for each of the three detector elements:

$$m \times (\lambda_{obs} - \lambda_{pred}) = A + B \times \lambda_{pred}, \tag{2}$$

where m is the spectral order, λ_{obs} the measured wavelength, λ_{pred} the theoretical wavelength including errors and with A and B as free parameters. This process was done for six different data sets of Capella. The constant B for the outer detector segments was $(1.32 \pm 0.10) \times 10^{-3}$ Å/Å and for the central segment $(0.56 \pm 0.03)\ 10^{-3}$ Å/Å.

Correction to the gap size between the outer and the central plates had to be applied. They are $(-22 \pm 3)\ 10^{-3}$ Å and $(-41 \pm 3)\ 10^{-3}$ Å, respectively. After applying all corrections, the wavelength uncertainty may be as low as 10 mÅ, supposing that the non-uniformities are stable in time.

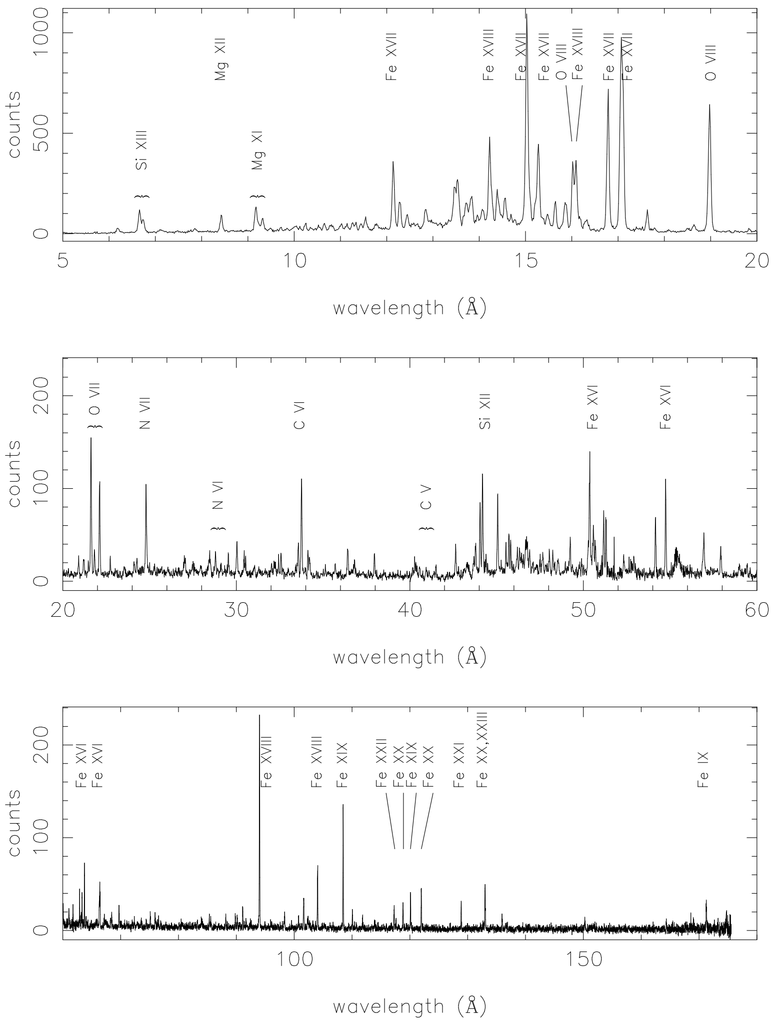

Figure 2. The complete LETGS spectrum of Capella, split into three parts for clarity. Note the difference in x and y scale for the three parts. Indicated in the plot are the triplets discussed in the text and a selection of the Fe lines at longer wavelengths.

5. LETG Efficiency

A much more difficult task is the determination of the effective area. During the telescope calibration performed at NASA-MSFC's long beamline XRCF, the instruments (HRMA, HRC-S, LETG) were calibrated separately but also in combination. In parallel, laboratory measurements together with theoretical models were used in order to improve the results (see Figure 3).

The transmission grating efficiency can be modeled in terms of the geometrical characteristics of the grating as, for instance, grating wire thickness, width, and the refractive index of the grating material. Particularly in wavelength bands where the wires are partially transparent, an exact knowledge of the wire cross section is important. It turns out that the assumption of a rectangular wire cross section (the simplest case) is not sufficient to explain the efficiency of a grating especially for higher diffraction orders. Throughout the whole development phase we have always adopted a trapezoidal rather than rectangular model. Then, depending on the transparency of the grating, the 'effective' width of the wires varies and the efficiency ratios among higher orders vary as well, exactly what is observed. This can

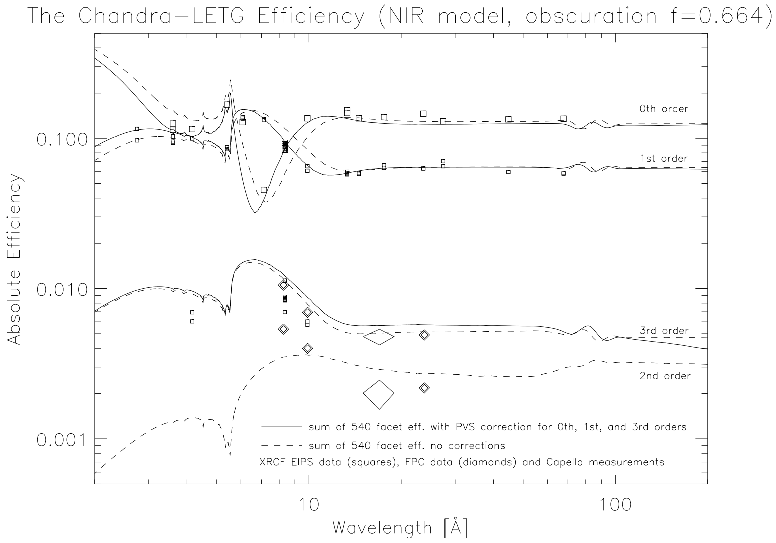

Figure 3. The absolute efficiency of LETG as a function of wavelength. So lid lines represent the theoretical model based on NIR-data of all 540 grating elements, dashed lines include corrections based on recent measurements using the PVS-gratings. Symbols represent XRCF measurements.

lead to a complicated behavior, particularly for those orders which are almost suppressed. The LETG gratings are designed to suppress the even orders which is achieved at a bar-slit ratio of 1:1. Due to uncertainties in the exact determination of the wire cross section and also slight inhomogeneities during the manufacturing process, the suppression works well for the second diffraction order but is extremely difficult to achieve for higher even orders.

At the beginning of the LETG program we realized that the testing of all grating samples (~3000, when AXAF still had 6 mirror shells and we were required to deliver a flight, a flight spare, and an engineering model) in the laboratory X-ray facility would be a horrendous task. Therefore we developed a novel method based on the transmissivity of a grating for polarized light in the so-called resonance domain, i.e., the wavelength range around the grating period (Lochbihler and Predehl 1992). This, in our case, is the NIR-region around $1\,\mu$m. This method was validated both by electron microscope studies and X-ray measurements on so-called 'Performance Verification Samples', ten randomly selected grating elements. Although the results of the complex tests at XRCF were not always easy to interpret, it became nevertheless apparent that there were significant deviations between model and data particularly at wavelengths between 7 and 10 Å. Deviations of up to 30% occurred. We therefore very accurately re-measured the PVS gratings in X-rays in an effort to re-calibrate the NIR-data. Based on this exercise, we have 'fudged' the NIR-data by adding small constants to the wire width, thickness and slope of the assumed mean trapezoidal cross sections of each grating. The most interesting result was that the thickness seems to depend on diffraction order. This suggests an underlying physical effect not considered so far. Combining all information from NIR, X-ray laboratory measurements, and XRCF calibration, we succeeded to establish an efficiency model for the LETG close to the required level of accuracy.

5.1. LETGS Effective Area

In order to establish the combined HRMA-LETG-HRC effective area, strong point sources with 'known' spectra have been chosen. For the long wavelength band beyond the Carbon edge, Sirius-B was considered to be the best candidate. According to existing white dwarf models (see Brinkman et al. 2000b for details) the flux uncertainty is smaller than 10%. The herewith derived effective area is therefore directly coupled to our knowledge of the Sirius B absolute flux.

The most straightforward way to verify the LETGS effective area is to use a continuum source with a well-defined spectrum. An additional difficulty is that the HRC-S cannot separate the different

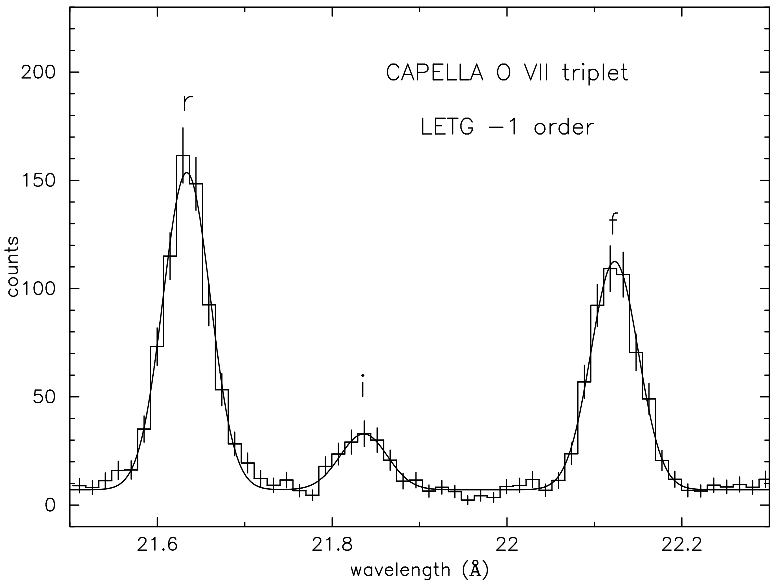

Figure 4. The Oxygen VII triplet in the LETGS –1 order spectrum with the resonance (r), the forbidden (f), and the intercombination (i) line. The measured ratios of these lines (from the fitted curve) are given in the text.

spectral orders. The predicted count rate therefore consists of the contributions of first and higher orders together. We are now in the process of applying this procedure to several celestial sources to look for systematic deviations, which can then be attributed to the LETGS-response. Also the comparison with HETG-ACIS-S measurements as well as observations using other spacecrafts such as XMM, SAX and ASCA are beeing used to cross calibrate our instrument.

6. Preliminary Capella Results

A quantitative analysis of the spectrum requires the exact knowledge of the effective area of the instrument over the entire wavelength band. However, some diagnostics based on intensity ratios of lines lying closely together could already be applied. A good example for line complexes are the helium-like triplets. Details of this preliminary analysis on this line complex and also on the resonance scattering in the Fe XVII 15 Å lines are given by Brinkman et al. 2000a.

The LETGS wavelength band contains the He-like triplets from C, N, O, Ne, Mg, and Si (wavelengths at roughly 40, 29, 22, 13.5, 9.0, and 6.6 Å, resp.). However, the Si and Mg triplet are not sufficiently resolved and the Ne IX triplet is too much blended with iron and nickel lines. The O VII lines are clean (see Figure 4) and the C V and N VI lines can be separated from the blends by simultaneously fitting all lines. These triplets are suited to diagnose plasmas in the density range $n_e = 10^8$–10^{11} cm^{-3} and corresponding temperature range $T \sim$ 1–3 MK. For the C, N, and O triplets the measured i/f ratios are [1] 0.38 ± 0.14, 0.52 ± 0.15, and 0.250 ± 0.35, respectively, which imply Pradhan(1982) densities n_e (in 10^9 cm^{-3}) $= 2.8 \pm 1.3, 6 \pm 3$, and $\lesssim 5$ (1σ upper limit), respectively, for typical temperatures as indicated by the $(i+f)/r$ ratios of 1, 1, and 3 MK, respectively. The derived densities are comparable to those of active regions on the Sun with temperatures of a few MK. Figure 4 shows a fit to the O VII triplet measured in the –1 order. The He-like triplet diagnostic, which was first applied to the Sun (e.g.,

[1] For the analysis we use a composite of six observations obtained in the week after first light, with a total observing time of 95 ksec.

Acton et al.(1972), McKenzie and Landecker(1982), Wolfson et al.(1983)) has now for the first time been applied to a star other than the Sun.

7. Conclusion

The Capella measurements with LETGS show a rich spectrum with excellent spectral resolution ($\Delta\lambda \simeq$ 0.06Å, FWHM). About 150 lines have been identified of which the brightest hundred are listed (see Brinkman et al. 2000b). The high-resolution spectra of the Chandra grating spectrometers allow us to carry out direct density diagnostics using the He-like triplets of the most abundant elements in the LETGS-band. This was so far only possible for the Sun.

References

Acton, L.W., Catura, R.C., Meyerott, A., Wolfson, C.J. 1972, Solar Phys., 26, 183

Brinkman, A.C., et al., 1987, Astroph. lett. & comm., Vol. 26, 73–80

Brinkman, A.C., et al., 1997, SPIE, 3113, 181–192

Brinkman, A.C., et al., 2000, ApJ , 530, 111

Brinkman, A.C., et al., 2000, SPIE, in press

Catura, R.C., Acton, L.W., and Johnson, H.M. 1975, ApJ , 196, L47

Dupree, A.K., Brickhouse, N.S., Doschek, G.A., Green, J.C., Raymond, J.C., 1993, ApJ , 418, L41

Hummel, C.A., Armstrong, J.T., Quirrenbach, A., Buscher, D.F., Mozurkewich, D., Elias, N.M. II, and Wilson, R.E., 1994, AJ, 107, 1859

Lochbihler H., Predehl P. 1992, Appl. Opt. 31, 964

McKenzie, D.L., Landecker, P.B. 1982, ApJ , 259, 372

Mewe, R., Heise, J., Gronenschild, E.H.B.M., Brinkman, A.C., Schrijver, J., den Boggende, A.J.F. 1975, ApJ , 202, L67

Mewe, R., 1991, A&A Rev., 3, 127

Mewe, R., Lemen, J.R., and Schrijver, C.J. 1991, Ap&SS , 182, 35

Murray, S.S., et al. 1997, SPIE, 3114, 11

Pradhan, A.K. 1982, ApJ , 263, 477

Predehl, P., et al., 1997, SPIE, 3113, 172–180

Schrijver, C.J., Mewe, R., van den Oord, G.H.J., and Kaastra, J.S. 1995, A&A , 302, 438

Van Speybroeck, L.P., Jerius, D., Edgar, R.J., Gaetz, T.J., and Zhao, P., 1997, SPIE, 3113, 89

Wolfson, C.J., Doyle, J.G., Phillips, K.J.H. 1983, ApJ , 269, 319